Physical Principles of Nanoparticle Cellular Endocytosis

Sulin Zhang,[†,‡,*] Huajian Gao,[§,*] and Gang Bao[∥,*]

[†]Department of Engineering Science and Mechanics, The Pennsylvania State University, University Park, Pennsylvania 16802, United States, [‡]Department of Biomedical Engineering, The Pennsylvania State University, University Park, Pennsylvania 16802, United States, [§]School of Engineering, Brown University, Providence, Rhode Island 02912, United States, and [∥]Department of Bioengineering, Rice University, Houston, Texas 77005, United States

ABSTRACT This review article focuses on the physiochemical mechanisms underlying nanoparticle uptake into cells. When nanoparticles are in close vicinity to a cell, the interactions between the nanoparticles and the cell membrane generate forces from different origins. This leads to the membrane wrapping of the nanoparticles followed by cellular uptake. This article discusses how the kinetics, energetics, and forces are related to these interactions and dependent on the size, shape, and stiffness of nanoparticles, the biomechanical properties of the cell membrane, as well as the local environment of the cells. The discussed fundamental principles of the physiochemical causes for nanoparticle–cell interaction may guide new studies of nanoparticle endocytosis and lead to better strategies to design nanoparticle-based approaches for biomedical applications.

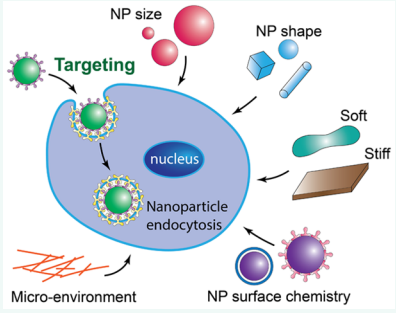

KEYWORDS: nanoparticles · endocytosis · nanomedicine · cellular uptake · ligand–receptor binding · coarse-grained model · membrane bending · membrane tension

The past decade has witnessed enormous research efforts undertaken in the development of nanosized particulate platforms for biological studies, early stage cancer detection, simultaneous diagnosis and treatment of pathological conditions, and targeted therapy with minimal toxicity to achieve "personalized" medicine.[1−12] To enable cell-type specific targeting, nanoparticles (NPs) are often surface-coated with biopolymers or macromolecules, bioconjugated with targeting ligands that bind specifically to the complementary receptors on the cell membrane. Armed with drug molecules and/or diagnostic reporters, the NPs may transport in the bloodstream, adhere to the endothelium, diffuse through the intercellular space, specifically adhere to the diseased cells, enter the cells *via* different pathways (Figure 1), and release the drug molecules effectively. Accordingly, the efficacy of NP-based agents depends on the efficiency of these subprocesses, many of which remain poorly understood. Instead of giving an exhaustive review on the research progress in all the subprocesess, this review sets forth to provide a theoretical foundation for the biophysics of NPs entry into the cells *via* endocytosis. The theoretical focus renders this review distinctive from and complementary to several existing reviews on similar topics that are primarily focused on either the novel concepts and experimental observations[13−15] or computational simulations.[16] It also significantly extends previous reviews on the mechanics of cell–NP interactions[17] and of vesicle wrapping NPs.[18] In particular, we probe the mechanical forces generated at the NP–cell interface and the kinetics and energetics of the NP–cell interactions. We then describe how the size, shape, elastic modulus and surface chemistry of NPs affect the interactions and consequently dictate the cellular uptake properties. The integrated theories presented here may form a basis for the rational design of NP-based diagnostic and therapeutic agents with improved targeting efficiency.

Depending on the particle size and surface treatment, engineered particles may enter cells *via* different pathways, as schematically shown in Figure 1. Micrometer-sized particles can enter the cells through phagocytosis[19] or macropinocytosis.[20,21] Phagocytosis (Figure 1a)

* Address correspondence to suz10@psu.edu, huajian_gao@brown.edu, gb20@rice.edu.

Received for review May 26, 2015 and accepted August 8, 2015.

Published online August 08, 2015
10.1021/acsnano.5b03184

directs the formation of cup-shaped membrane protrusions that gradually surround and close the particles. The shape and size of the phagosomes, *i.e.*, the closed membrane protrusions, are dictated by the particles being taken up (typically a few micrometers). Phagocytosis is primarily used to uptake dead cells, cell debris, and pathogens. Macropinocytosis (Figure 1b) is an actin-regulated process that involves engulfment of a large quantity of extracellular fluid and particles through plasma membrane ruffling. The membrane ruffles exhibit different shapes, and when close, form large organelles called macropinosomes.[19] Because of the micrometer length scale of phagocytosis and macropinocytosis, actin assembly plays an imperative role in the uptake process.[21,22] In clathrin-mediated endocytosis (Figure 1d), receptor−ligand binding triggers the recruitment and formation of "coated pits" (clathrin) on the cytosolic side of the plasma membrane.[23] The pits self-assemble into closed polygonal cages that facilitate the endocytosis. Clathrin assembly is also responsible for the formation of vesicle necking and the pinch-off process in the late stage of membrane wrapping of NPs. Clathrin-mediated endocytosis is the most common endocytic pathway exploited by viruses.[24,25] Caveolin-dependent endocytosis (Figure 1c) involves the assembly of the hairpin-like caveolin coats on the cytosolic side of the plasma membrane, forming a flask-shaped caveolae of ~50−80 nm in diameter.[26,27] It is generally known that Clathrin- and Caveolin-dependent endocytosis involves complex biochemical signaling cascades.[28] However, to what extent the entry of engineered NPs is regulated by the biochemical signaling remains poorly understood. While clathrin and caveolin provide additional driving force for endocytosis, clathrin and caveolin independent endocytosis[29,30] (Figure 1e) can also occur through receptor−ligand binding. NPs without conjugated ligands may be endocytosed through non-specific interactions as well (Figure 1f). For large NPs, transmembrane penetration may occur provided the interaction force is sufficiently large.[31−35] This process, however, may be harmful to cells since large membrane pores must open for particle entry. Small NPs and molecules (<1 nm) may enter the cell by simply diffusing across the lipid bilayer (Figure 1g).

With the rapid advance of nanotechnology, NPs of different types can now be synthesized with well-controlled size uniformity and shape (Table 1), many of which have manifested a great potential for a broad range of biomedical applications including *in vitro/vivo* diagnostics,[36] cell tracking,[37] molecular imaging,[38−41] and drug/gene delivery.[42−44] These NPs have a common core/coating structure. The cores are either inorganic or organic, while the coating layer is generally formed by natural macromolecules, synthetic biopolymers or their

VOCABULARY: **Membrane wrapping** - the action that cell membrane curves to wrap around an object; **Endocytosis** - the process that cell membrane wraps around an object and takes it inside the cell; **Adhesion Strength** - measures how strong two surfaces cling together; **Ligand density** - refers to the number of ligands per unit area; **Entropy** - a thermodynamical quantity that measures the disorder of a system; **Enthalpy** - defined as a thermodynamic potential that consists of the internal energy of the system plus the product of pressure and volume of the system; **Coarse-grained model** - a simulation model that uses pseudoatoms (coarse grains) to represent groups of atoms, instead of explicitly representing every atom in the system; **Molecular dynamics simulation** - a computer simulation of physical movements of atoms and molecules; **Bending energy** - the energy stored in an object when it is curved; **Deformation** - the action or process of changing in shape of an object through the application of force

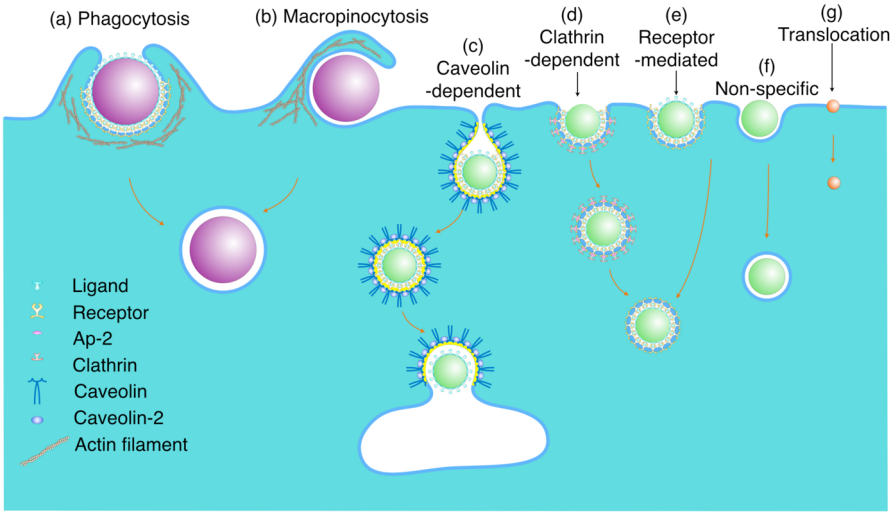

Figure 1. Possible internalization pathways of NPs.

TABLE 1. Various Types of NPs as Diagnostic and/or Therapeutic Agents

NP type	size range	typical shapes
Metallic	5—500 nm	Sphere/cube/rod
Oxides	5—200 nm	Sphere/cube
Quantum dot	2—30 nm	Sphere/ellipsoid
Silica	10—100 nm	Sphere
Carbon nanotube	1—10 nm	Cylinder
Graphene	10—1000 nm	2D sheet
Polymer	10—1000 nm	Spherical/cylindrical/rod-like/elliptical/cubic/disk-like
Nanogel	10—1000 nm	Cylinder
Liposome	100—1000 nm	Spherical
Bacteria	500—5000 nm	Rod/spirals/ellipsoid
Dendrimers	1—100 nm	Spherical
Micelles	10—100 nm	Spherical/rod-like/worm-like/cylindrical/elliptical
Virus	10—300 nm	Icosahedral/spherical/filament/rod

combinations. The coating layer renders NPs water-dispersible, prevents aggregation, reduces nonspecific adsorption in biological systems, and provides a platform for conjugation of targeting ligands or other functional molecules (such as a chelator). The length, charge, hydrophobicity, and flexibility of the coating molecules,[45] and the overall size, shape, and elastic modulus of the NPs are critical mediators for the *in vitro* and *in vivo* performance of NPs.[41,46,47]

Bioconjugated NPs in many aspects are biomimics of viruses,[30,48,49] which represent the most relevant nanoscale objects in nature to artificial nanomedicine. Just as engineered NPs, viruses are typically of size from 10 to 300 nm, feature a diverse collection of shapes ranging from icosahedral to spherical to filaments to bullet/rod, and are coated with ligands on their surfaces. Many viruses, such as HCV[50] and influenza,[29] enter host cells *via* protein-mediated endocytosis,[24,25,51,52] are replicated inside the host cells, and exit from the host cells *via* exocytosis (known as budding). While viral entry is a highly active process involving a set of biochemical signaling, budding,[53,54] in contrast, is largely passive and can be regarded as the reverse process of endocytosis of synthetic NPs. The high efficiency and specificity of viruses have stimulated enormous research efforts to uncover the physical principles harnessed by the evolutionary design of viruses, which can conveniently lend to engineer NPs for disease targeting. For example: How fast does viral entry/budding occur? How many replicated viruses can simultaneously bud out from host cells? Why viral entry/budding is size selective and shape sensitive? Why are that many ligands needed for viral entry/budding and what if the virus is a few ligands less or more? Does nature design *via* evolution the number of ligands and the size/shape such that these parameters work in concert for virus infection? Does local biomechanical environment influence viral entry? Answering similar fundamental questions in the cellular uptake of synthetic NPs will pave the way toward the development of better principles for the biomimetic design of highly effective NPs.

NP—CELL MEMBRANE INTERACTIONS: FORCES AND ENERGETICS

When a NP docks on cell membrane, it forms a highly heterogeneous NP—cell interface and initiates dynamic physiochemical interactions and a sequence of kinetic processes. The interaction forces of different origins shape the interactions, modify the associated energy landscapes, and dictate the endocytosis of the NPs.[55] Wrapping NPs necessitates curving the cell membrane and pulling the membrane against membrane tension to the wrapping site, presenting resistance to endocytosis. All the other forces, including electrostatic, van der Waals (vdW), hydrophobic forces, ligand—receptor binding *etc.*, can be lumped together as the adhesion force that drives endocytosis. The adhesion force can stem from either specific or nonspecific interactions, or both.[56] Specific interactions involve recognition and binding of the ligands coated on the NP surface to the complementary receptors on the cell membrane. Analogous to a molecular key-and-lock system, ligand—receptor binding enforces targeting specificity of NPs. All the other interactions are nonspecific, which generate an overall attraction or repulsion between molecules and generally affected by ionic strength and pH.

Specific interactions differ from nonspecific interactions in at least three distinct features, which have profound implications in the uptake kinetics. First, unlike nonspecific interactions in which the driving force is spontaneously in action when a NP docks onto the cell membrane, specific interaction through ligand—receptor bindings introduces a time delay: wrapping necessitates diffusion of the receptors to the binding sites, thereby setting a characteristic time scale of endocytosis.[57,58] Second, much like cleavage fracture (or crack healing) in crystals that involves discrete bond breaking (or formation),[59,60] ligand—receptor binding proceeds in a discrete manner. As the chemical energy release (the driving force) is only available after each discrete membrane unit (the area covered by each ligand) wraps the NP, an energy barrier between two consecutive binding events arises from membrane bending and tension.[53] The wrapping area and hence the energy barrier in each discrete step can be tailored by the spacing of the ligands (*i.e.*, the ligand density) coated on the NP surface. This barrier further delays wrapping, but the relevant time scale is thought to be shorter by several orders of magnitude than that of the receptor diffusion. However, when the coated ligands are sparse, the barrier becomes non-negligible. Third, receptors, in addition to providing adhesion force, also carry translational entropy.[61—63] Wrapping is thus

no longer a local event but global in nature as it causes redistributions of the receptors on the entire cell membrane. Concentration of receptors to the NP surface through ligand−receptor binding involves entropic penalty. The dual character (releases chemical energy upon binding and at the same time carries entropy) renders the adhesion strength in receptor-mediated endocytosis a variable quantity,[63−66] in distinct contrast to the adhesion strength in nonspecific uptake that is locally defined.

During wrapping, membrane bends away from its intrinsically curved state characterized by the spontaneous curvature κ_0. The spontaneous curvature arises from the asymmetry of the lipid bilayers and/or the presence of asymmetrically shaped transmembrane proteins in general, and the assembly of the protein coats in particular in the case of clathrin and caveolin dependent endocytosis. The bending energy density (per unit area) is quantified by $1/2B(\bar{\kappa} - \kappa_0)^2$, where B is the membrane bending stiffness, $\bar{\kappa} = (\kappa_1 + \kappa_2)/2$ is the mean curvature of the membrane, and κ_1 and κ_2 are the two principal curvatures of the NP surface. To pull the surrounding membranes toward the site for wrapping, work against membrane tension needs to be done. Cells may actively modulate their membrane tension under different physiological conditions through various mechanisms, for instance, membrane reservoir release.[67] Membrane wrapping first activates the release of membrane reservoirs during which membrane tension remains nearly constant. Once the excess membrane area is used out, the membrane elastically extends to further wrap the NP during which membrane tension increases.

The coupling between membrane bending and stretching in the wrapping process complicates the calculation of the membrane deformation energy. For a partially wrapped NP with a wrapping extent η (the areal ratio of the wrapped and the total surface area of the NP), the deformation energy consists of three contributions: the bending energy $C(\eta)$ and the stretching energy $\Gamma(\eta)$ stored in the membrane segment wrapped onto the NP (the black line segment in Figure 2), and the additional deformation energy $\Lambda(\eta)$ (including both bending and stretching) stored in the curved membrane detaching from the contact to the NP[68,69] (the green line segment in Figure 2). For spherical NP, $C(\eta) \sim \eta$, and $\Gamma(\eta) \sim \eta^2$, and $\Lambda(\eta)$ is generally a nonlinear function of η. The total membrane deformation energy at the degree of wrapping η ($0 \leq \eta \leq 1$) is the sum of the three components: $W(\eta) = C(\eta) + \Gamma(\eta) + \Lambda(\eta)$. Determining $\Lambda(\eta)$ generally requires numerically calculating the equilibrium shapes of the membrane segment,[68,69] but becomes trivial under two special conditions: for a fully wrapped NP ($\eta = 1$), the host membrane sets back to its original curvature at this special stage, and $\Lambda = 0$; under the tensionless condition, $\Lambda(\eta) = \Gamma(\eta) = 0$ for all η since the equilibrium membrane profile is a catenoid, a minimal surface with zero mean curvature.

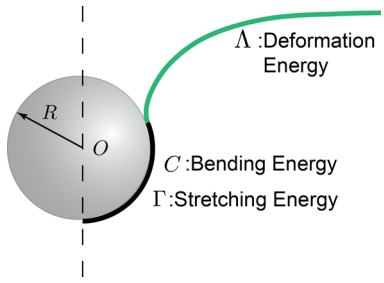

Figure 2. Membrane deformation energies when wrapping a NP.

Membrane curves locally but gets tensed globally. A characteristic length scale that weighs the relative significance of bending and stretching energies characterizes the locality of an event: $\lambda = (2B/\sigma)^{1/2}$,[68] where σ is the membrane tension. For typical values of $B = 15k_BT$, $\sigma = 0.05$ *m*N/m, one finds $\lambda \approx 50$ nm. For NP radius $R < \lambda$, bending dominates the wrapping process and membrane tension is negligible; as R increases from λ, membrane tension effect becomes progressively more pronounced.

CELLULAR UPTAKE OF SPHERICAL NPS: SIZE EFFECT

When Can a NP be Endocytosed? Given a spherical NP of radius R, a first question one asks is whether it can be internalized by the cell. We begin with a simple case in which nonspecific adhesion is the only driving force for membrane wrapping. The total adhesion energy supplied for fully wrapping the NP ($\eta = 1$) is $4\pi R^2\alpha_{ns}$, where α_{ns} is the adhesion strength. Assuming a vanishing spontaneous curvature ($\kappa_0 = 0$), the bending energy for fully wrapping the NP is $C = 8\pi B$, independent of NP size, and the stretching energy is $\Gamma = 4\pi R^2\sigma$. Balancing the adhesion energy and membrane deformation energy defines a lower limit of the NP radius below which the NP cannot be endocytosed

$$R_{min} = \sqrt{2B/(\alpha_{ns} - \sigma)} \quad (1)$$

As $R_{min} < \lambda$ generally holds, the effect of membrane tension is negligible, and $R_{min} \approx (2B/\alpha_{ns})^{1/2}$. Considering a typical value of membrane bending rigidity $B \sim 15\ k_BT$, and of the nonspecific adhesion strength $\alpha_{ns} \sim 1\ k_BT/nm^2$, $R_{min} \sim 5$ nm. NPs smaller than R_{min} may enter the cells by other pathways, such as translocation (Figure 1g). It is also possible that several small NPs may agglomerate into a cluster through membrane curvature mediated attraction.[70] The agglomerated NP cluster may well exceed the lower size limit, and thereby be able to be internalized together.[71] One notes from eq 1 when $\alpha_{ns} = \sigma$, $R_{min} \rightarrow \infty$, a condition under which endocytosis will never occur regardless of its size because the adhesion energy is fully paid to the stretching energy, leaving none to pay the curvature

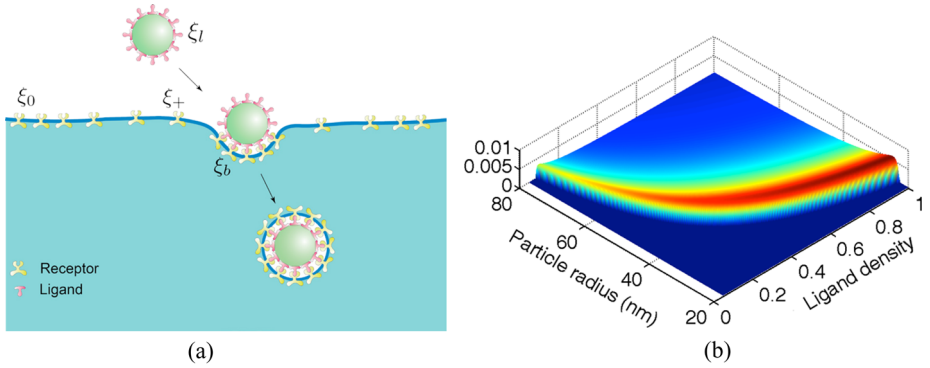

Figure 3. (a) Schematic illustration of membrane wrapping of a single NP, driven by ligand−receptor binding. Wrapping depletes the receptors in the near vicinity of the NP, creating a receptor concentration gradient that drives the diffusion of the receptors from the remote region to the binding sites. (b) Interrelated effect of NP size and ligand density on the endocytic time of a NP.[66] Reproduced from ref 66. Copyright 2010 American Physical Society.

energy. As pointed out previously, the self-regulated rest membrane tension by cells is usually small. However, with increasing NP size, wrapping the NP would put the membrane in increasingly high tension. Thus, there also exists an upper limit of NP radius beyond which endocytosis does not occur either.[72] This upper limit ought to be at the same length scale of the cell.

In the case that membrane wrapping is primarily driven by specific interaction, the adhesion strength can be partitioned into two components:[64,65] $\alpha_s = \alpha_h + \alpha_r$, where α_h and α_r are the enthalpic and entropic components, respectively. The enthaplic component is provided by the ligand−receptor binding, $\alpha_h = \mu\xi_b$, where μ is the chemical energy release upon the binding of a ligand−receptor pair and ξ_b is the receptor density bound to the NP surface (see Figure 3a). Note that in the case that every receptor binds to a ligand on the NP surface (one-to-one corresponding binding), ξ_b reaches its maximum, ξ_l, the density of ligands coated onto the NP surface. Nonspecific interaction can be lumped into enthalpic adhesion strength by adopting an effective μ_{eff}. The entropic term, α_r, always negative, depends on the local receptor density. A reasonable approximation gives rise to $\alpha_r = \ln(\xi_+/\xi_l)$, where ξ_+ is the receptor density in the depletion zone near the NP (see Figure 3a). Assuming at the minimal NP radius the number of receptors consumed by wrapping is insignificant, causing negligible redistribution of receptors. One then approximates $\xi_+ \sim \xi_0$, the receptor density at the remote region. Neglecting membrane tension, the energy balance defines a lower limit of the NP radius for the case of specific interaction:

$$R_{min} = \sqrt{2B/[\mu\xi_l + \ln(\xi_0/\xi_l)]} \qquad (2)$$

One notes a singular condition $\alpha_h = |\alpha_r|$ exists under which endocytosis is not possible (as $R_{min} \to \infty$) because recruiting receptors to wrapping the NP is entropically too expensive. The singular condition implies an upper NP radius (with a fixed ligand density) beyond which wrapping is source (receptor)-limiting.

How Fast Can a NP Be Endocytosed? Once a NP exceeds the minimal size, endocytosis becomes thermodynamically possible. An immediate question that follows is the time duration for completing endocytosis. To see this, we note that the wrapping rate is limited by several barrier-crossing events. As pointed out previously, an energy barrier arises due to the discreteness of ligand−receptor binding. With a detailed calculation of the deformation energy landscape of membrane wrapping of a NP at different wrapping extents η, Deserno identified another energy barrier that separates the partially and fully wrapped states, indicating the transition is nonspontaneous.[68,69] For typical values of σ = 0.05 mN/m, R = 30 nm, and $B = 20k_BT$, the barrier can be as high as $\Delta E = 40\ k_BT$, which is too high to be thermally crossed. Wrapping can thus be kinetically trapped at a partially wrapped state. The energy barrier scales with the membrane tension and vanishes in the tensionless condition. Increasing the adhesion strength beyond a certain value diminishes the barrier as well.

When the adhesion strength and the ligand density are sufficiently high, the time scales associated with the above-mentioned two barrier crossing events are generally considered to be shorter than that of receptor diffusion, and the wrapping rate is predominantly limited by the receptor diffusion. Upon a NP docking on the cell membrane, binding of the receptors to the surface ligands of the NP depletes the receptors in the vicinity of the NP, forming a depletion zone with a reduced receptor density. The concentration gradient of receptors drives diffusion of the receptors from the remote region to the depletion zone, making subsequent wrapping possible. To quantify the endocytic time, Gao *et al.*[57] have developed a front-tracking diffusion model that couples conservation of receptors and chemical potential balance of the receptors in the

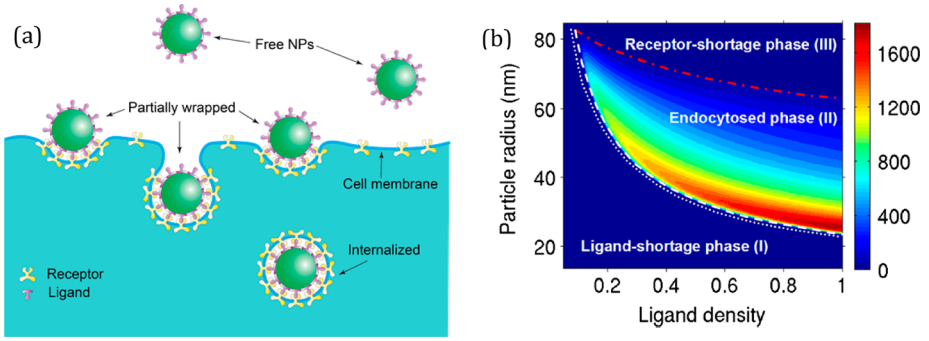

Figure 4. Simultaneous entry of multiple NPs. (a) Schematics. (b) Phase diagram of cellular uptake in the space of particle size and ligand density. Reproduced from ref 66. Copyright 2010 American Physical Society.

depletion zone and on the NP surface. The model predicted that the endocytic time is NP size dependent, as

$$t_w = \beta R^2/D \quad (3)$$

where D is the diffusivity of the receptors, and β is dimensionless, but dependent on R, referred to as the "speed factor". The speed factor can be analytically calculated for cell membrane of infinite size wrapping a spherical or a cylindrical NP. With physiologically relevant parameters, the model identified an optimal NP size of 27−30 nm in radius at which the endocytic time is the shortest.

The scaling law can also be followed from the conservation of receptors,[57,58,66] which defines a characteristic length scale of the impact region L from which receptors are depleted for wrapping: $\pi L^2 \xi_0 = 4\pi R^2 \xi_l$. For all the receptors to diffuse and bind to the surface ligands of the NP, the wrapping time is then $t_w \sim L^2/D \sim R^2 \xi_l / D\xi_0$. This scaling analysis also reveals that the endocytic time correlates positively with the ligand density but negatively with the receptor densities on the cell membrane.

These above analyses assumed that every ligand binds to a receptor in wrapping the NP, *i.e.*, one-to-one corresponding binding. However, in the case of densely coated ligands on the NP surface and high ligand−receptor affinity, wrapping may proceed with some ligands unbound to receptors. This is beneficial as far as the endocytic time is concerned because fewer receptors are required, but detrimental due to the loss of targeting specificity. A thermodynamic model by Yuan *et al.* predicts the binding density of the receptors relative to the ligand density on the NP surface[66]

$$\hat{\xi} \equiv \xi_b/\xi_l \sim 1 - e^{-\hat{\kappa}} \quad (4)$$

Here, $\hat{\kappa} = 2B/R^2\xi_l$ is the curvature energy in the unit area covered by each ligand. Clearly from eq 4, one-to-one corresponding binding ($\hat{\xi} = 1$) occurs only when the unit bending energy $\hat{\kappa}$ is sufficiently large. For a sufficiently large NP (thus relatively small $\hat{\kappa}$) but fixed ligand density ξ_l, $\hat{\xi}$ can be significantly smaller than 1. Under this condition, membrane wrapping may proceed with many ligand missed by receptors. Yuan *et al.* further predicts the speed factor for wrapping a spherical NP:[66]

$$\beta = 4\hat{\xi}\xi_l/(\xi_0 - \xi_+) \quad (5)$$

where $\xi_+ = e^{-\mu}\hat{\xi}/(1-\hat{\xi})$. On the basis of eq 5, a phase diagram of $1/t_w$ can be constructed in the space of the two controlling parameters, NP radius R and ligand density ξ_l, as shown in Figure 3b. One identifies a lower phase boundary below which $t_w \to \infty$ and an upper phase boundary beyond which the same limit occurs. The lower phase boundary is enthalpically governed, as defined in eq 1, and the upper phase boundary is entropically governed, as in eq 2. Between these two extreme conditions, there exists an optimal condition at which the endocytic time minimizes, corresponding to the ridgeline in the phase diagram. At the saturated ligand density, the optimal NP radius for the shortest endocytic time is ~25 nm, which agrees well with the prediction of the front-tracking diffusion model[57] and previous experimental data.[73,74]

How Many NPs Can Be Taken up by a Cell? Another problem, equally important to the endocytic time of a single NP, is the cellular uptake of NPs by cells. The total cellular uptake of NPs matters for a range of biomedical applications of NPs, including the maximum drug dosage that can be reached when the NPs are used for drug delivery, or the signal intensity when the NPs are used for intracellular imaging and disease diagnosis.

When the cell in *in vitro* experiments is immersed in culture medium loaded with dispersed NPs of a bulk density φ, the system eventually reaches a steady state with finite cellular uptake.[71,75,76] The steady state can be regarded as a thermodynamic equilibrium at which a total of n NPs are associated with the cell. Of the n NPs, some are wrapped by the cell membrane with different degrees of wrapping;[63,64] some are internalized, as schematically shown in Figure 4a. The exact partition of the NPs is driven by the chemical potential difference between the NPs that are bound to the cell membrane, those suspended in the solution and internalized into the cell. The cell membrane is also partitioned into two parts: a free, planar membrane region and a curved membrane region bound to the NPs.

The energetics description of multiple NP−membrane interactions remains nearly the same as in single NP endocytosis for either nonspecific or specific interactions, with the only added entropics of NP distribution. Equating the chemical potential of the NPs in the bulk solution and on the cell membrane gives rise to the cellular uptake (the total number of endocytosed NPs):[64,65]

$$N = A\phi e^{4\pi R^2[\alpha_M - w(\eta=1)]} \quad (6)$$

where A is the surface area of the cell accessible by the NPs, α_M is the adhesion strength and the superscript "M" denotes the case of multiple NP entry, and $w(\eta = 1) = 2B/R^2 + \sigma$ is the membrane deformation energy density (per unit area) at the fully wrapped state $\eta = 1$.

Figure 4b plots the phase diagram of the cellular uptake in the space of NP radius and ligand density driven by specific interactions. Similar to the phase diagram for the endocytic time in Figure 3b, there exists a lower and an upper bound of the cellular uptake, with the enthalpic and entropic origins, respectively, as previously discussed. Indeed, one notes from eq 6 that N is small when the adhesion energy is insufficient to pay the membrane deformation penalty: $\alpha_M \leq w(\eta = 1)$. This follows essentially the same lower bound dictated by eq 1. Increasing the NP size and/or ligand density intensifies the competition for receptors by the NPs,[77,78] leading to increasingly high entropic cost and thus decreased α_M. This entropic limit corresponds to the upper bound defined by eq 2. The phase diagram also identifies a small region (the red region) within which cellular uptake is maximized. This region corresponds $\sim R \in (25, 30)$ and $\xi_l \in (0.8, 1)$, with a total cellular uptake of a couple of thousand for physiologically relevant parameters. Both the range of the predicted total cellular uptake and the optimal range of NP size agree with the experimental data.[71,74,75]

The Optimal Condition. From an energetics viewpoint, multi-NP entry is mechanistically similar to single-NP endocytosis. The energy balance of single-NP endocytosis remains to be met in multi-NP entry, giving rise to the same enthalpically regulated lower phase boundary. Irrespective of a single NP or multi-NPs, wrapping consumes receptors and is thus source-limiting, leading to the same entropically modulated upper phase boundary. It should be pointed out that in the case the NPs in multi-NP entry are spatially too close on the cell membrane such that their membrane curvature-mediated interactions[70] are not negligible, the lower phase boundary may deviate from that of single-NP endocytosis. Nevertheless, the same mechanisms regulating the phase boundaries for the endocytic time and cellular uptake allow us to define a nominal cellular uptake rate,[79] as

$$\Theta(R; \xi_l) = N/t_w \quad (7)$$

Noticeably, the optimal conditions for the shortest endocytic time (Figure 3b) and highest cellular uptake (Figure 4b), and hence Θ, are similarly close to the lower phase boundary: $R^2\xi_l = 2B/\mu$. Indeed, both the ridgelines follow a hyperbolic fitting: $n_{opt} \approx 4\pi R^2\xi_l$, where n_{opt} is the optimal number of ligands coated on NP surface. This is not surprising: once the number of ligands coated onto the NP surface exceeds the minimal value, the energy balance condition is met. Coating additional ligands is no longer beneficial, but only increases the number of receptors required for wrapping and thus intensifies the competition for receptors among NPs, leading to longer wrapping time and less cellular uptake. Given the biophysically relevant ranges for membrane bending rigidity (10−40 k_BT) and receptor−ligand binding energy μ (10−20 k_BT), the optimal number of ligands n_{opt} ($\approx 8\pi B/\mu$) coated onto NPs falls in the range ~10−100, irrespective of the NP size. The extensively studied model system, the Semliki Forest virus (SFV), is about 35 nm in radius, covered with 80 glycoproteins (ligands),[80,81] which appears to follow the optimal condition.

The above energetics analysis suggests that tailoring enthalpics and entropics shift the phase boundaries and modifies the cellular uptake. For sufficiently large NPs, the cortical actin network may play a resisting role in endocytosis.[82] This factor may be taken into account by simply defining an effective bending rigidity B_{eff}. Nonspecific interactions, including hydrophobic, electrostatic and van der Waals interactions, may also contribute to additional adhesion energy. Lumping the specific and nonspecific interactions together defines an effective ligand−receptor binding energy, μ_{eff}. A relative variation of both B_{eff} and μ_{eff} alters the enthalpics and hence the lower bound of the phase diagrams.[79] On the other hand, increasing receptor population (*i.e.*, increasing ξ_0) lowers the entropic penalty for the receptors to bind with NPs, and hence shifts the upper bound upward. A high bulk density of NPs φ in solution yields a high surface concentration of NPs on cell membrane, leading to intensified competition for receptors among adhering NPs and high entropic penalty.[77,78] This follows that increasing φ shifts the upper bound of the uptake rate downward. One further notes that the effect of membrane tension is negligible for small NPs but significant for large NPs. This follows that membrane tension primarily regulates the upper bound of the uptake rate, but hardly affects the lower bound.[79]

SHAPE EFFECT

Nonspherically shaped NPs are also widely used in biomedical diagnostics and therapeutics. Their potential nanotoxicities have also attracted much attention. Typical 1D nanomaterials include nanotubes, nanowires, and filamentous bacteria with radius at the

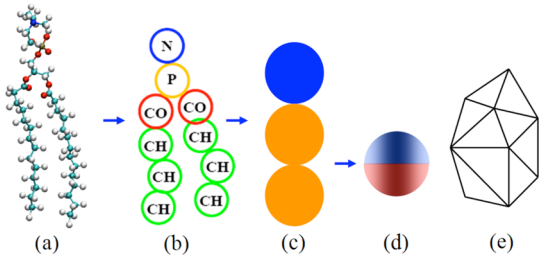

Figure 5. Simulation models of lipids at different length scale. (a) All-atom model of the DMPC lipid molecules; (b and c) CG models, a 10-agent[92] (b) and a 3-agent[93,94] (c) CG model; and a one-agent-thick membrane model[95] (d). (e) Triangulated membrane model.[89,90]

nanoscale but length at a much larger scale; typical 2D nanomaterials are plate-like materials with thickness at the nanoscale but lateral dimensions at a much larger scale, including mica nanosheets, boron nitride nanosheets, and graphene-family nanomaterials, as listed in Table 1. For 3D nonspherical NPs, their three dimensions are comparable. For all these nonspherical nanomaterials, the fundamental biophysics of cell−NP interactions established for spherical NPs remains valid. However, owing to their asymmetrical geometries, they exhibit unique wrapping modes during endocytosis.[83−88]

Coarse-Grained Models. The energetics of endocytosis of a nonspherical NP is complicated by the symmetry breaking of cell membrane deformation morphology, for which the deformation energy is analytically nontrivial, particularly when membrane tension is nonnegligible. To investigate the effects of NP shape on the kinetics of endocytosis, computational modeling at different length scales provides a powerful alternative. Since the length and time scales involved in NP endocytosis are on the order of 100 nm or more, and milliseconds to minutes, respectively, they are typically beyond the reach of the full-atom molecular dynamic (MD) simulations (Figure 5a). To the other end of the length spectrum, the triangulated membrane simulation models[89,90] (Figure 5e) spatially discretize membrane into triangles in the general framework of Helfrich theory.[91] However, these continuum models suffer from additional numerical burden in addressing lateral diffusion of lipids and receptors, which is the key factor dictating the time scale of endocytosis.

To gain a molecular-scale understanding of NP targeting, it is essential to develop multiscale models that link interactions on the molecular level and NP absorption/uptake by the cells at the subcellular level. Coarse-grained (CG) methods[92−100] (Figure 5b−d) have gained popularity for their flexibility and diversity. CG models typically involve grouping a cluster of atoms into a single CG agent, thereby reducing the total number of the degrees of freedom by several orders of magnitude, and accordingly improving the computational affordability. Such CG approaches vary in their level of details, depending on the number of agents per lipid and complexity of the inter-agent interactions. Early CG models for lipid bilayers used explicit solvents that are also coarse-grained. As the solvent occupies a 3D volume, the associated degrees of freedom outnumber those of the 2D lipid bilayers, and the majority of the computational cost goes to the solvent, rather than the lipid bilayer. Thus, CG models with implicit solvent are particularly attractive. Stabilizing the coarse-grained lipid bilayer in a 2D fluid phase and under solvent-free condition with physiologically relevant membrane properties was numerically nontrivial. Varying such solvent-free CG models need to use complicated multibody potentials to achieve biophysically relevant membrane properties. Solvent-free CG models with simple pairwise potentials have only been recently developed; of particularly noteworthy are the 3-bead model by Cooke *et al.*[93,94] and the one-agent-thick model by Yuan *et al.*[95] These models are computationally highly efficient while biophysically faithful to the underlying molecular interactions in a wide range of membrane-mediated processes, including endocytosis.

The one-agent-thick lipid bilayer model[95] (Figure 5d) coarse-grains the lipid membrane as a single layer of agents that are self-assembled into a 2D fluid surface in a solvent-free environment. The inter-agent interaction potential is anisotropic but of a pairwise form, composed of two functions that separately control the distance and orientation dependence. The model membrane properties are highly tunable through only four key model parameters that control separately the lipid diffusivity, bending and area compression moduli, and spontaneous curvature, respectively. The simple interaction potential can lead to robust self-assembly of randomly distributed agents in 3D space into 2D fluid membranes. Through careful mapping to the membrane bending modulus and the in-plane lipid diffusivity, the in-plane agent dimension of our model is found to be ~0.5 nm and the basic time scale of our model is ~0.1 μs. Both the length and time scales are at least one order of magnitude higher than other solvent-free CG models.[92,99,100] The model was successfully applied to study homogeneous vesicle shape transformation under osmotic conditions,[101] protein-mediated lipid sorting and domain coarsening of ternary membranes,[102] and red blood cell disorders.[103,104]

Simultaneous Rotation and Wrapping of 3D Nonspherical NPs. Huang *et al.*[83] adopted the one-agent-thick membrane model to characterize the endocytic mode of spherocylindrical NPs with different aspect ratios. In this model, NP surface is also coarse-grained to discrete agents, some representing ligands (see Figure 6a−c). The lipid membrane is made to be tensionless by scaling the membrane area in the CGMD simulations. The aspect ratio of the spherocylindrical NPs is defined

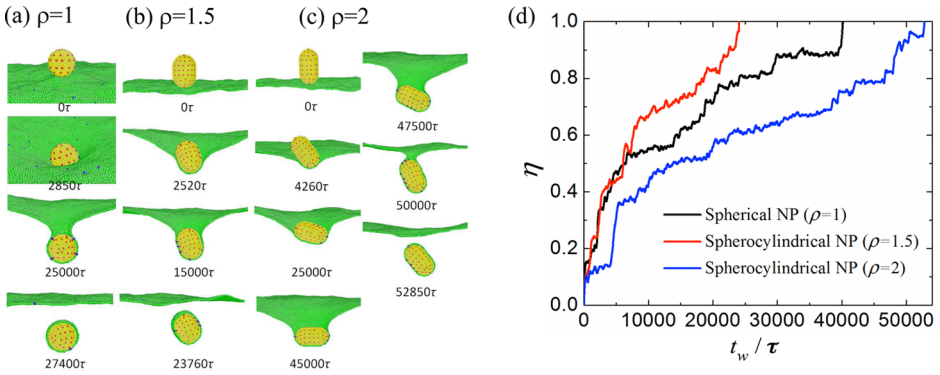

Figure 6. (a−c) Simulation snapshots of the endocytic process of spherocylindrical NPs with different aspect ratios. For all the cases shown, R = 14 nm. (a) ρ = 1; (b) ρ = 1.5; (c) ρ = 2. Here, τ is a characteristic time scale of the model. Color-coded beads represent different coarse-grained constituents. Green, lipids; blue, receptors; yellow, ambient NP surface; red, ligands. (d). Shape effects on the endocytic time of NPs. Evolution of the areal wrapping fraction of NPs with the same radius (R = 10.0σ) but different aspect ratios. In the simulations, the spherocylindrical NPs are initially docked on the membrane with their long axes perpendicular to the membrane. Reprinted from ref 83. Copyright 2013 American Chemical Society.

by $\rho = (R + 0.5L)/R$, where R and L are the radius of the hemispherical caps at both ends and the length of the cylindrical portion, respectively. In the simulations, the spherocylindrical NPs are initially docked on the pre-equilibrated membrane, with their long axes normal to the membrane surface (θ = 90°). Figure 6a−c depicts the snapshots of the endocytic process of the NPs with three different aspect ratios, ρ = 1, 1.5, and 2. Note ρ = 1 represents a spherical NP. All the three NPs can be completely endocytosed through a general process involving membrane invagination, membrane necking and pinch-off.

Distinct entry modes are observed in the wrapping process of the spherocylindrical NPs, as shown in Figure 6a−c. For ρ = 1, wrapping is accompanied by NP rotation. For ρ = 1.5, the NP tilts by an angle of ~20° from its initial upright docking position once wrapping begins. Membrane wrapping of the NP then proceeds at this angle until the NP is fully internalized. The invagination of the NP with a larger aspect ratio (ρ = 2) involves two symmetry-breaking processes. At the initial wrapping stage, the NP rotates until it completely lays down on the membrane surface with its long axis. The NP then stands up and is finally endocytosed with a nearly 90° entry angle. Such a lying-down-then-standing-up sequence appears to be universal for spherocylindrical NPs with ρ > 2. If the initial docking angle θ = 0° with the long axis parallel to the membrane surface, the NP would simply stand up and then be endocytosed.

At prescribed ligand density and NP radius and assuming one-to-one corresponding binding of ligand−receptor pairs, the endocytic time is proportional to the total number of receptors required for fully wrapping the NP. One then follows the scaling law: $t_w \sim \rho$. However, from the CGMD simulations by Huang *et al.*,[83] the spherical NP takes longer time to be fully endocytosed than the spherocylindrical NP of ρ = 1.5, but shorter time than the spherocylindrical NP of ρ = 2, as shown in Figure 6d. Further increasing ρ leads to increasing endocytic time, obeying the scaling law. This nonmonotonic behavior may be due to the distinct entry modes from spherical to spherocylindrical shape transitions. The scaling law and the simulation results indicate frustrated uptake of NPs with very high aspect ratios, such as 1D nanorods.

The wrapping energy landscape explains the sequence of simultaneous membrane wrapping and rotation during the internalization of a spherocylindrical NP. Figure 7a plots the curvature energy profiles for the NP (ρ = 2) as a function of the wrapping extent η, as if the NP were wrapped with a fixed entry angle, θ = 0° (horizontally) or θ = 90° (vertically). The analytical energy profiles, denoted by solid lines, agree very well with the CGMD simulations, denoted by symbols. For horizontal wrapping (θ = 0°) the curvature energy linearly scales with the wrapped areal fraction. For vertical wrapping (θ = 90°), the energy profile is constituted of three linear curves with different slopes. Since the two wrapping angles represent the extremes, the curvature energy profiles of all the other wrapping angles are enveloped by these two curves. The energy profiles indicate the sequence of membrane wrapping and NP rotation. At a small wrapping extent (η < 0.5), the relatively smaller curvature energy for θ = 0° suggests that an initially vertically docked or titled (0° < θ < 90°) NP would tend to lay down by rotation, *i.e.*, aligning its long axis with the membrane surface. Once η > 0.5, the NP would tend to stand up to gain a larger wrapping angle θ since wrapping with a large angle involves a smaller energy penalty. Upon completion of rotation, the NP would be wrapped with this angle until it is completely endocytosed. Thus, an initially vertically docked NP would take a laying-down-then-standing-up sequence to complete endocytosis, as schematically shown in Figure 7b.

The laying-down-then-standing-up wrapping sequence is consistent with the CGMD simulations for capped multiwalled carbon nanotubes (MWCNTs) by

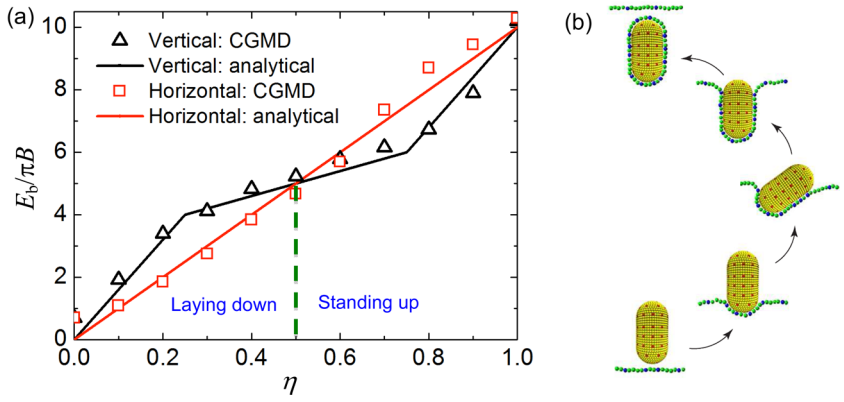

Figure 7. (a) The bending energy profile for internalizing a spherocylindrical NP (ρ = 2) with different wrapping angles explains the laying-down-then-standing-up process. (red: θ = 0°; black: θ = 90°.). (b) Schematics of the laying-down-to-standing-up process. Images reprinted or adapted from ref 83. Copyright 2013 American Chemical Society.

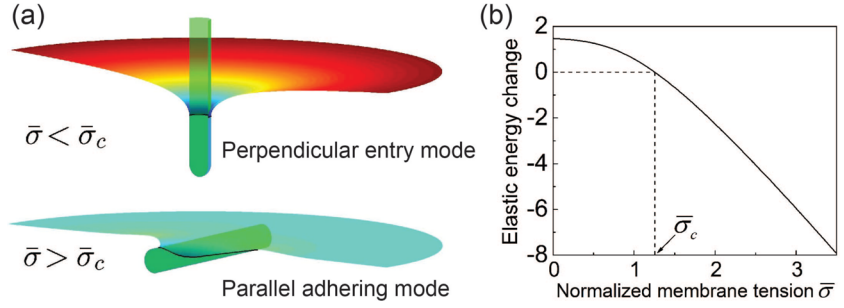

Figure 8. (a) Two modes of interaction between a cell membrane and a nanotube.[88] Reproduced from ref 88. Copyright 2014 American Chemical Society. (b) Elastic energy change as a function of the normalized membrane tension $\bar{\sigma}$, where $\bar{\sigma}_c = 2\pi/5$ is the critical point of transition between these two interaction modes.

Shi *et al.*[84] using the 3-agent lipid model and the accompanying experimental observations. A very long capped CNT can be considered as a 1D rod, the limiting geometry of the spherocylindrical NPs. The simulations demonstrated that at a relatively low receptor density the CNT rotates and is internalized with an entry angle close to 90°, exhibiting a tip-entry phenomenon. Also consistent to the analysis in Figure 7a, the rotation is driven by the relaxation of the deformation energy in the membrane during wrapping.

The tip rotation from a kinetics point of view by noting two relative time scales involved in the endocytosis of the CNTs, as pointed out by Shi *et al.*:[84] the wrapping time controlled by receptor diffusion and the NP rotation time controlled by the torsional force. In the case of physiologically relevant receptor density, wrapping is the limiting process compared to rotation. Thus, the NP has sufficient time to rotate so as to fully relax the deformation energy to achieve tip entry. On the contrary, in the case of very high receptor density, receptors are always immediately available for wrapping and wrapping would proceed very fast, leaving no time for rotation to occur. Under this condition, the NP is endocytosed with a low entry angle and tip entry becomes less predominant.[105]

Uptake of 1D and 2D Nanomaterials. Compared with the endocytosis of 3D nanorods whose interaction mode exhibits a lying-down-then-standing-up sequence as identified in Figures 6 and 7, recent work has revealed two fundamental modes of interaction between a 1D nanomaterial and the cell membrane: a perpendicular entry mode and a parallel adhering mode (see Figure 8a).[88] Theoretical analysis showed that these two basic modes are controlled by a single dimensionless parameter, the normalized membrane tension $\bar{\sigma} = 2\sigma R^2/B$ with R being the radius of the 1D nanomaterial. From an energetic point of view, $\bar{\sigma}$ represents the relative ratio of the membrane stretching and bending energies in the total elastic energy of the membrane. The membrane bending energy tends to rotate the nanotube to a perpendicular entry angle while the membrane stretching energy prefers a vanishingly small entry angle. When $\bar{\sigma}$ falls below a critical value $\bar{\sigma}_c$ ($\bar{\sigma} < \bar{\sigma}_c$), the membrane bending energy dominates over the stretching energy and the 1D nanomaterial rotates to a high entry angle during uptake. For $\bar{\sigma} > \bar{\sigma}_c$, the 1D nanomaterial is driven by the dominating stretching energy toward a low entry angle and eventually adheres to the membrane surface in a near-parallel configuration (see Figure 8b). This $\bar{\sigma}$-governed uptake behavior is ubiquitous in the interactions between 1D nanomaterials and cell membranes, and the theory can be employed to understand many biological phenomena such as the regulation of filopodia

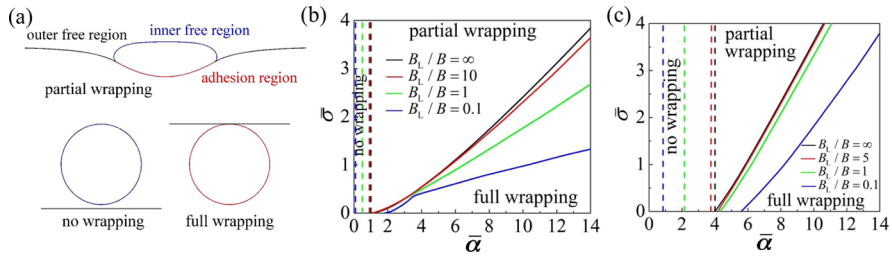

Figure 9. (a) Schematic of typical wrapping states and (b and c) wrapping phase diagrams with respect to normalized adhesion energy and membrane tension $\bar{\sigma}$ at different values of the rigidity ratio B_L/B, where B_L is the bending rigidity of the liposome; (b) 2D case; (c) 3D case. Dashed lines, boundaries between no wrapping and partial wrapping states; solid lines, boundaries between partial and full wrapping states. Adapted with permission from ref 106. Copyright 2011 American Physical Society.

radius and the instability of microtubules confined by cell membranes.[88]

The reason why the receptor-mediated endocytosis of nanorods exhibit a single interaction mode of a lying-down-then-standing-up sequence (Figure 7), while that of 1D nanomaterials exhibits two interaction modes depending on the scaled membrane tension $\bar{\sigma}$ could be understood as follows. Note that receptor-mediated endocytosis is usually regarded as a process limited by the diffusion of receptors in the cell membrane toward the contact region.[57] The membrane wrapping of the curved tip of a 1D nanomaterial is governed by 2D diffusion of receptors in the membrane plane, while the wrapping of the cylindrical wall is regulated by 1D diffusion of receptors. This means that the tip, rather than the lateral wall, of a 1D nanomaterial should be wrapped first. As long as the specific energy of receptor−ligand interaction can overcome the membrane deformation energy penalty induced by the tip wrapping, the subsequent interaction should be controlled by the two tension-dependent interaction modes.[88] In comparison, for short nanorods with two curved tips and a much smaller lateral wall, the difference between receptor diffusion between the tip and wall regions is not as evident. Therefore, the wrapping of short nanorods would be mainly governed by the elastic energy of the deformed membrane that adopts the lying-down-then-standing-up sequence to reduce the membrane deformation energy.

Depending on their size, geometry and surface properties, 2D nanomaterials can exhibit several different configurations in the cellular interaction.[85] Recently, a theoretical analysis has been performed to study two modes of interaction between the cell membrane and a rigid 2D nanomaterial: near-perpendicular transmembrane penetration and parallel attachment onto a membrane. It was shown that the splay (bending) and membrane tension energies serve as the main driving force for the near-perpendicular (parallel) configuration of a transmembrane (membrane attaching) 2D nanomaterial.[87] As 2D nanomaterials enter the cells typically not *via* endocytosis but other pathways, their internalization mechanisms are not detailed here.

UPTAKE OF SOFT NPS

For soft NPs with comparable bending modulus as the lipid bilayer, such as vesicles, liposomes, micelles, polymeric capsules, and NPs coated with long polymers, both the cell membrane and the NP itself deform. The partition of the total deformation energy into the cell membrane and the NP alters the energy landscape, giving rise to different kinetics of endocytosis. During the wrapping process, the NP deforms into different shapes, thus the effect of elastic modulus is inherently coupled with the shape effect.

Yi *et al.*[106] developed a theoretical model concerning the endocytosis of a fluid vesicular NP such as a liposome in the framework of Helfrich theory. By solving the equilibrium shape equations of the cell membrane as well as the vesicular NP, the total deformation energy of the system can be obtained at different wrapping extents (see Figure 9a). Their energetics analyses showed that endocytosis is very sensitive to the relative stiffness of the NP to the cell membrane, as shown in the phase diagram of the scaled membrane tension $\bar{\sigma}$ and adhesion energy density $\bar{\alpha} = 2\alpha R^2/B$, where α is the adhesion energy density (see Figure 9b,c). As NP becomes softer, the transition lines separating from partial to fully wrapping shift downward, indicating endocytosis is more difficult to complete. The result that stiff vesicular NPs can achieve full wrapping more easily than soft NPs has been confirmed recently in a combination of experiments and molecular dynamics simulations on the cell uptake of core−shell NPs with a lipid shell.[107] Similar elasticity effects have also been observed in the cell uptake of spherical solid nanocapsules[108] and (2D cylindrical) nanorods. It was found that solid nanocapsules require less adhesion energy to achieve full wrapping than fluid vesicular NPs with the same bending stiffness.[108]

To explain why softer NP is more difficult to be endocytosed, one observes that cell membrane wets soft NPs once they dock on the cell membrane, as shown in Figure 9a. The softer the NP is, the larger the wetting angle, and the higher extent of spreading of the NP on the cell membrane. The highly spread NP forms large curvatures at the spreading front. Further wrapping the

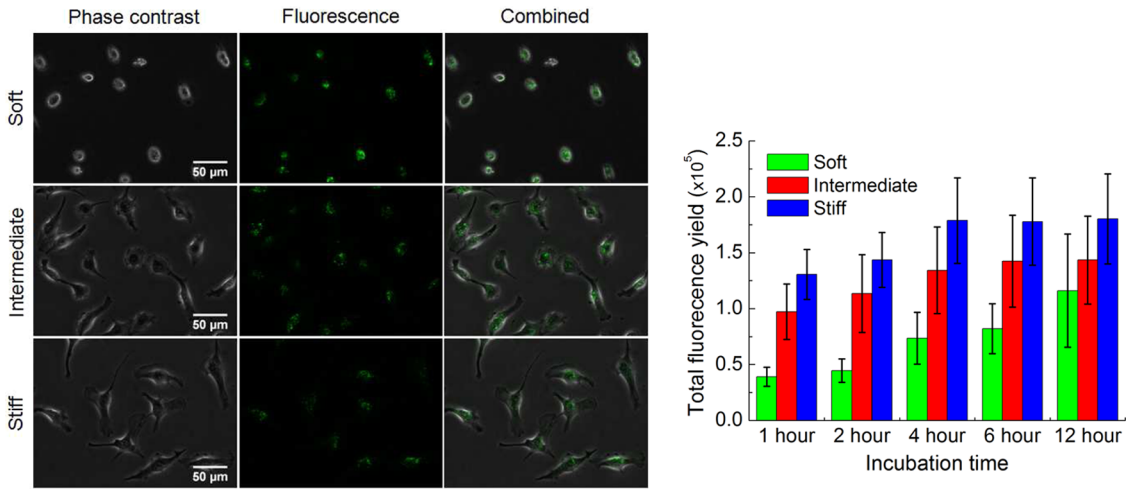

Figure 10. Left: Cellular uptake of the fluorescent NPs by the cells on polyacrylamide substrates of varying stiffness. Cells were cultured on substrates for 12 h before loading the NPs. Images were taken after loading the NPs for 6 h. Right: The total fluorescence yield of individual cells on the polyacrylamide substrates of varying stiffness obtained by multiplying fluorescence per unit area by the projected cell area on a cell by cell basis.[117] The difference between any two groups at any specified time point of measurement is statistically significant ($p < 0.01$ using Student t test). Reproduced from ref 117. Copyright 2013 American Chemical Society.

NP involves overcoming a very large bending energy barrier inherent to the spread shape. The energy barrier may be sufficiently large to completely stall the wrapping. Interestingly, Yi *et al.*[106] noted that many viruses exploit the stiffness to facilitate the infectious process: they soften before uptake *via* fusion, while harden before budding out of the host cells *via* exocytosis.

LOCAL MECHANICAL ENVIRONMENTAL EFFECTS

Our previous analyses reveal that cellular uptake of NPs depends on not only the size, shape and chemophysical properties of NPs, but also the biomechanical properties of cell membrane, including membrane tension and bending modulus. In parallel to the theoretical and computational studies, numerous *in vitro* experiments[71,75,109,110] have been carried out to assess the delivery efficiency of NPs and provided rich data sets for validating the theoretical and computational models. However, in these *in vitro* experiments the cells were exclusively cultured on glass or plastic substrates, which are both mechanically stiff and topographically flat. In contrast, the ECMs *in vivo* are soft and consist of fibrils such as collagens. These discrepancies raise an immediate concern regarding to what extent the *in vitro* experimental results are transferrable to *in vivo* conditions. It has well established from the study of mechanobiology[111−116] that local physical cues of various kinds modulate cell responses, resulting in changes in cell morphology and surface mechanics, which may in turn affect the cellular uptake of NPs.

To characterize the role of local physical environment on the cellular uptake of NPs, Huang *et al.*[117] carried out *in vitro* studies with different characteristics of cell culture substrates. In a first study, polyacrylamide (PA) hydrogels of varying stiffnesses, soft (Young's modulus: 1.61 ± 0.11 kPa), intermediate (3.81 ± 0.12 kPa), and stiff (5.71 ± 0.51 kPa) were used in the *in vitro* experiments to explore the effect of substrate stiffness on the cellular uptake.[117] Bovine aortic endothelial cells (BAECs) were cultured on the gels for 12 h before loading fluorescent polystyrene NPs (100 nm) into the culture medium. The seemingly small difference in the gel stiffness is sufficient to induce changes in cell morphology, as shown by the phase contrast images (Figure 10, left). Endocytosis was driven by nonspecific interactions, since the NPs are not conjugated with antibodies. The *in vitro* experiments confirmed that substrate stiffness plays a significant role in altering the cellular uptake of NPs. The total fluorescence yield per cell was measured at different times after NPs were loaded, indicating the uptake level of NPs. With increasing substrate stiffness, the cellular uptake per cell increases (Figure 10, right), but the cellular uptake per cell surface area decreases (not shown here).[117]

Using poly(methyl methacrylate) (PMMA) fibrous substrates fabricated *via* electrospinning, Huang *et al.*[118] further explored the effects of substrate topography, characterized by the fibril density, on the cellular uptake of NPs. Substrates of three types of topographies, flat PMMA surface, and sparse and dense PMMA fibrous substrates, were used. The responses of human osteosarcoma SaOS-2 cells to substrate topography were investigated using fluorescence microscopy by simultaneously staining F-actin, vinculin, and cell nuclei, as shown in Figure 11 (left). The 100 nm fluorescent polystyrene NPs were again used to assess the cellular uptake. Figure 11 (right) shows that the cellular uptake

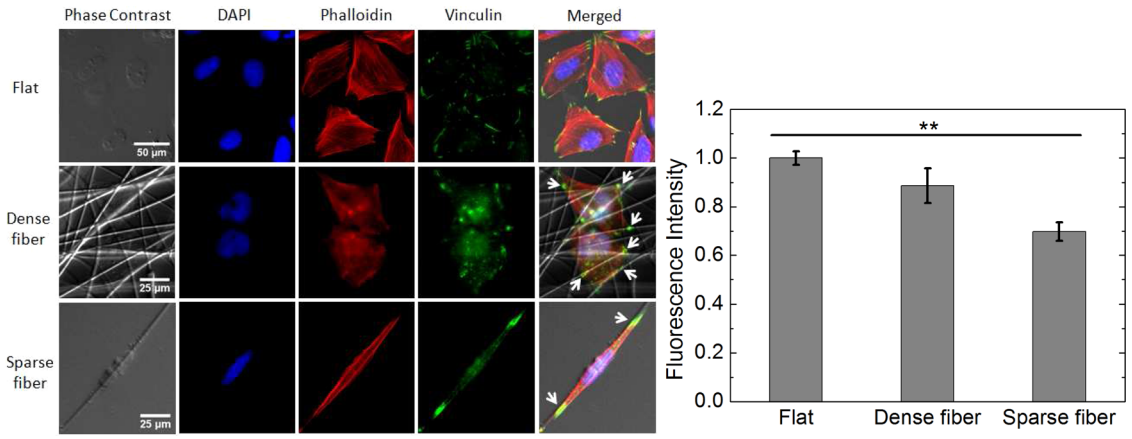

Figure 11. Left: Representative fluorescence images of SaOS-2 cells on various substrates with distinct surface topographies. Right: Cellular uptake of fluorescent NPs by cells on substrates of different surface topographies. The fluorescence intensities are normalized by the intensity on flat PMMA surface.[118] **Significance at $p < 0.01$ between any two groups. Reproduced with permission from ref 118. Copyright 2015 Wiley & Sons, Inc.

of NPs on sparse fibrous substrates was reduced by about 30% as compared with the cells on the flat PMMA substrates.

The regulative role of substrate stiffness and topography on the cellular uptake stems from the altered mechanical properties of cell membrane and the cell spreading area, as indicated by eq 6. First, substrate stiffness modulates the mechanical properties of cell membrane. Recent MD simulation results suggested that the fluorescence lifetime of DiI chromophores embedded in lipid bilayer is an effective indicator of relative membrane tension,[119] which was confirmed in experiments.[120] Indeed, fluorescence lifetime measurements of DiI-C_{12} within cells demonstrated that cell membrane is less tense on softer PA gels.[117] This predicts that the cellular uptake of cells on softer PA gels or denser fibrous substrates is higher on a per membrane area basis. Second, substrate stiffness modulates cell spreading. The stiffer the substrate is, the larger the spreading area of the cell.[117] As shown in eq 6, the cellular uptake linearly scales with the surface area of the cell membrane, since it represents the assessable area to the NPs. It turns out that the cell surface area is dominant factor over the membrane tension effect, and hence, the cellular uptake on a per cell basis increases with increasing substrates stiffness.

The observed effect of substrate topography on the cellular uptake can be explained by the same principle. First, fluorescence lifetime measurements of DiI-C_{12} showed that cell membrane on sparse fibrous substrate is more tensed than those on flat and dense fibrous substrates; membrane tension of cells on the latter two substrates is comparable.[118] The spreading area of cells on flat substrate is nearly 2-fold higher than that of cells on fibrous substrates, whereas the spreading areas of the cells on dense and sparse fibrous substrates are comparable.[118] Since the cell surface area is the dominant factor over the membrane tension effect, the cellular uptake on flat substrate is the highest. For cells on fibrous substrates, the higher membrane tension renders lower cellular uptake by cells on sparse fibrous substrate than on dense fibrous substrate.

CONCLUSION AND PROSPECTIVE OUTCOME

The NP−cell interface is highly heterogeneous, generating forces of different origins that shape the energy landscape of NP−cell interactions. These forces are determined by a suite of variables inherent to the NPs and the cells (size, shape, stiffness, surface chemistry of the NPs, elasticity of the cell membrane, and receptor diffusivity, *etc.*), rendering cellular uptake NP size selective, shape sensitive, and stiffness dependent. As cell morphologies and surface mechanics are dependent on the local microenvironment and disease states, cellular uptake of NPs may not only be cell type specific, but also tissue-environment and disease state specific.

It is clear that the effects of key parameters important to the cellular uptake are strongly interrelated, as exemplified by the phase diagrams in the space of NP radius and ligand density. The interrelated effects define a narrow window in the parametric space within which the cellular uptake is optimized. In addition to the interplay between NP size and ligand density, many other interrelated effects are yet to be quantified. For example, when a soft NP is being wrapped, its shape dynamically changes, *i.e.*, the effects of NP stiffness and shape are coupled and interrelated. The interrelated effects indicate that improving one parameter may adversely impact another, making the search of the optimal parametric window experimentally cost-ineffective. Coarse-grained modeling discussed here will continue to be a powerful tool to define the complex interrelations.

Challenges remain to identify the most efficient targeting strategy suitable and specific to diseased tissues. Chemotargeting is currently the most popular targeting strategy, wherein NPs conjugated with ligands target cell surface receptors that are specific

to the diseased cells. Such an active targeting method has been proven efficient so long as unique receptors can be identified and are overexpressed on diseased cells compared with normal cells. The work reviewed here provide compelling evidence that mechanical properties of the cells and the NPs can also bias the cellular uptake of NPs, which suggests a new targeting strategy, mechanotargeting. Given that mechanical properties of many tumors are different than those of the normal tissues, mechanotargeting is complementary to chemotargeting and may be useful in achieving more effective cancer diagnosis and treatment. This opens up a new paradigm for the design of NP-based nanomedicine with improved targeting selectivity and reduced toxicity.

To facilitate a unifying understanding, this review aims to provide a coarse-grained picture on the interaction forces that mediate the cellular uptake of NPs. Namely, all the atomic and molecular forces are lumped into driving (adhesion) and resistance forces without differentiating their atomic and molecular origins. Noting that endocytosis is essentially a multiscale process initiated by single protein conformational changes and subsequently involving large-scale membrane deformation; therefore, information regarding how the atomic and molecular scale events trigger the cellular level functions could be lost due to the coarse-grained treatment. For example, to ensure targeting specificity, tethered ligands on the NP surface necessarily adopt appropriate conformations so as to be recognized by and accessible to the cell-surface receptors. A single parameter, *i.e.*, ligand−receptor binding affinity, may not suffice to describe the conformational changes of the proteins during the binding events. Further advancement of highly targeted NP-based therapy may hinge upon the quantitation of the interaction forces at the atomic and molecular levels and linking the atomic and molecular events to cellular functions. We expect that multiscale modeling coupling different length and time scales will play an important role in this aspect.

To date, clinical application of NPs is still hampered by frequent high-uptake in the liver, systematic toxicity of the carriers, and insufficient selectivity and uptake by tumor and/or cancer cells. From a biomimetic point of view, the current state-of-the-art design of NP-based therapeutics remains far less efficient than nature-synthesized NPs—viruses and bacteria. Numerous studies have made it clear that the extremely efficient and robust biological processes, such as viral infection and white cell attacking bacteria, come with the sophisticated ways that living system harnesses physical principles. Further design of smart, multifunctional biomimetic NPs necessitates continuing unraveling the underlying biophysics of the biological counterparts.

Conflict of Interest: The authors declare no competing financial interest.

Acknowledgment. S.L.Z. gratefully acknowledges supports from the National Science Foundation (NSF) grants (Career Award: CMMI-0754463/0644599; CBET-1067523) and the National Institutes of Health (NHLBI R21 HL122902). H.J.G. acknowledges supports from NSF (CMMI-1028530 and CBET-1344097). G.B. acknowledges supports from the National Institutes of Health as an NHLBI Program of Excellence in Nanotechnology Award (HHSN268201000043C to G.B.) and an NIH Nanomedicine Development Center Award (PN2EY018244 to G.B.). We are also grateful to Mr. Peng Zhao at Penn State University for producing a few images of endocytosis in this manuscript.

REFERENCES AND NOTES

1. Liu, X.; Dai, Q.; Austin, L.; Coutts, J.; Knowles, G.; Zou, J.; Chen, H.; Huo, Q. A One-Step Homogeneous Immunoassay for Cancer Biomarker Detection Using Gold Nanoparticle Probes Coupled with Dynamic Light Scattering. *J. Am. Chem. Soc.* **2008**, *130*, 2780–2782.
2. Mani, V.; Chikkaveeraiah, B. V.; Patel, V.; Gutkind, J. S.; Rusling, J. F. Ultrasensitive Immunosensor for Cancer Biomarker Proteins Using Gold Nanoparticle Film Electrodes and Multienzyme-Particle Amplification. *ACS Nano* **2009**, *3*, 585–594.
3. Stoeva, S. I.; Lee, J. S.; Smith, J. E.; Rosen, S. T.; Mirkin, C. A. Multiplexed Detection of Protein Cancer Markers with Biobarcoded Nanoparticle Probes. *J. Am. Chem. Soc.* **2006**, *128*, 8378–8379.
4. Qian, X.; Peng, X.-H.; Ansari, D. O.; Yin-Goen, Q.; Chen, G. Z.; Shin, D. M.; Yang, L.; Young, A. N.; Wang, M. D.; Nie, S. *In Vivo* Tumor Targeting and Spectroscopic Detection with Surface-Enhanced Raman Nanoparticle Tags. *Nat. Biotechnol.* **2008**, *26*, 83–90.
5. Nie, S.; Xing, Y.; Kim, G. J.; Simons, J. W. Nanotechnology Applications in Cancer. *Annu. Rev. Biomed. Eng.* **2007**, *9*, 257–288.
6. Moghimi, S. M.; Hunter, A. C.; Murray, J. C. Nanomedicine: Current Status and Future Prospects. *FASEB J.* **2005**, *19*, 311–330.
7. Peer, D.; Karp, J. M.; Hong, S.; FaroKhzad, O. C.; Margalit, R.; Langer, R. Nanocarriers as an Emerging Platform for Cancer Therapy. *Nat. Nanotechnol.* **2007**, *2*, 751–760.
8. Petros, R. A.; DeSimone, J. M. Strategies in the Design of Nanoparticles for Therapeutic Applications. *Nat. Rev. Drug Discovery* **2010**, *9*, 615–627.
9. Wang, M.; Thanou, M. Targeting Nanoparticles to Cancer. *Pharmacol. Res.* **2010**, *62*, 90–99.
10. Yezhelyev, M. V.; Gao, X.; Xing, Y.; Al-Hajj, A.; Nie, S.; O'Regan, R. M. Emerging Use of Nanoparticles in Diagnosis and Treatment of Breast Cancer. *Lancet Oncol.* **2006**, *7*, 657–667.
11. Fischer, H. C.; Chan, W. C. W. Nanotoxicity: The Growing Need for *in Vivo* Study. *Curr. Opin. Biotechnol.* **2007**, *18*, 565–571.
12. Kim, B. Y. S.; Rutka, J. T.; Chan, W. C. W. Current Concepts: Nanomedicine. *N. Engl. J. Med.* **2010**, *363*, 2434–2443.
13. Albanese, A.; Tang, P. S.; Chan, W. C. W. The Effect of Nanoparticle Size, Shape, and Surface Chemistry on Biological Systems. *Annu. Rev. Biomed. Eng.* **2012**, *14*, 1–16.
14. Canton, I.; Battaglia, G. Endocytosis at the Nanoscale. *Chem. Soc. Rev.* **2012**, *41*, 2718–2739.
15. Chou, L. Y. T.; Ming, K.; Chan, W. C. W. Strategies for the Intracellular Delivery of Nanoparticles. *Chem. Soc. Rev.* **2011**, *40*, 233–245.
16. Ding, H.-m.; Ma, Y.-q. Theoretical and Computational Investigations of Nanoparticle-Biomembrane Interactions in Cellular Delivery. *Small* **2015**, *11*, 1055–1071.
17. Gao, H. Probing Mechanical Principles of Cell-Nanomaterial Interactions. *J. Mech. Phys. Solids* **2014**, *62*, 312–339.
18. Bahrami, A. H.; Raatz, M.; Agudo-Canalejo, J.; Michel, R.; Curtis, E. M.; Hall, C. K.; Gradzielski, M.; Lipowsky, R.; Weikl, T. R. Wrapping of Nanoparticles by Membranes. *Adv. Colloid Interface Sci.* **2014**, *208*, 214–224.
19. Swanson, J. A. Shaping Cups into Phagosomes and Macropinosomes. *Nat. Rev. Mol. Cell Biol.* **2008**, *9*, 639–649.

20. Lewis, W. H. Pinocytosis. *Bull. Johns Hopkins Hosp.* **1931**, *49*, 17–27.
21. McNeil, P. L. Mechanisms of Nutritive Endocytosis. Iii. A Freeze-Fracture Study of Phagocytosis by Digestive Cells of Chlorohydra. *Tissue Cell* **1984**, *16*, 519–533.
22. Mooren, O. L.; Galletta, B. J.; Cooper, J. A. Roles for Actin Assembly in Endocytosis. *Annu. Rev. Biochem.* **2012**, *81*, 661–686.
23. Roth, T. F.; Porter, K. R. Yolk Protein Uptake in the Oocyte of the Mosquito Aedes Aegypti. *J. Cell Biol.* **1964**, *20*, 313–332.
24. Marsh, M.; Helenius, A. Virus Entry: Open Sesame. *Cell* **2006**, *124*, 729–740.
25. Mercer, J.; Schelhaas, M.; Helenius, A. Virus Entry by Endocytosis. *Annu. Rev. Biochem.* **2010**, *79*, 803–833.
26. Palade, G. E. An Electron Microscope Study of the Mitochondrial Structure. *J. Histochem. Cytochem.* **1953**, *1*, 188–211.
27. Yamada, E. The Fine Structure of the Gall Bladder Epithelium of the Mouse. *J. Cell Biol.* **1955**, *1*, 445–458.
28. Cavalli, V.; Corti, M.; Gruenberg, J. Endocytosis and Signaling Cascades: A Close Encounter. *FEBS Lett.* **2001**, *498*, 190–196.
29. Lakadamyali, M.; Rust, M. J.; Zhuang, X. W. Endocytosis of Influenza Viruses. *Microbes Infect.* **2004**, *6*, 929–936.
30. Sieczkarski, S. B.; Whittaker, G. R. Influenza Virus Can Enter and Infect Cells in the Absence of Clathrin-Mediated Endocytosis. *J. Virol.* **2002**, *76*, 10455–10464.
31. Ding, H. M.; Tian, W. D.; Ma, Y. Q. Designing Nanoparticle Translocation through Membranes by Computer Simulations. *ACS Nano* **2012**, *6*, 1230–1238.
32. Wong-Ekkabut, J.; Baoukina, S.; Triampo, W.; Tang, I. M.; Tieleman, D. P.; Monticelli, L. Computer Simulation Study of Fullerene Translocation through Lipid Membranes. *Nat. Nanotechnol.* **2008**, *3*, 363–368.
33. Yang, K.; Ma, Y. Q. Computer Simulation of the Translocation of Nanoparticles with Different Shapes across a Lipid Bilayer. *Nat. Nanotechnol.* **2010**, *5*, 579–583.
34. Zhang, H.; Ji, Q.; Huang, C.; Zhang, S.; Yuan, B.; Yang, K.; Ma, Y.-q. Cooperative Transmembrane Penetration of Nanoparticles. *Sci. Rep.* **2015**, *5*, 10525.
35. Lin, J.; Alexander-Katz, A. Cell Membranes Open "Doors" for Cationic Nanoparticles/Biomolecules: Insights into Uptake Kinetics. *ACS Nano* **2013**, *7*, 10799–10808.
36. Josephson, L.; Perez, J. M.; Weissleder, R. Magnetic Nanosensors for the Detection of Oligonucleotide Sequences. *Angew. Chem., Int. Ed.* **2001**, *40*, 3204–3206.
37. Lewin, M.; Carlesso, N.; Tung, C.-H.; Tang, X.-W.; Cory, D.; Scadden, D. T.; Weissleder, R. Tat Peptide-Derivatized Magnetic Nanoparticles Allow *in Vivo* Tracking and Recovery of Progenitor Cells. *Nat. Biotechnol.* **2000**, *18*, 410–414.
38. Lee, J.-H.; Huh, Y.-M.; Jun, Y.-w.; Seo, J.-w.; Jang, J.-t.; Song, H.-T.; Kim, S.; Cho, E.-J.; Yoon, H.-G.; Suh, J.-S.; et al. Artificially Engineered Magnetic Nanoparticles for Ultra-Sensitive Molecular Imaging. *Nat. Med.* **2007**, *13*, 95–99.
39. Gao, X. H.; Cui, Y. Y.; Levenson, R. M.; Chung, L. W. K.; Nie, S. M. *In Vivo* Cancer Targeting and Imaging with Semiconductor Quantum Dots. *Nat. Biotechnol.* **2004**, *22*, 969–976.
40. Nahrendorf, M.; Jaffer, F. A.; Kelly, K. A.; Sosnovik, D. E.; Aikawa, E.; Libby, P.; Weissleder, R. Noninvasive Vascular Cell Adhesion Molecule-1 Imaging Identifies Inflammatory Activation of Cells in Atherosclerosis. *Circulation* **2006**, *114*, 1504–1511.
41. Tong, S.; Hou, S.; Zheng, Z.; Zhou, J.; Bao, G. Coating Optimization of Superparamagnetic Iron Oxide Nanoparticles for High T2 Relaxivity. *Nano Lett.* **2010**, *10*, 4607–4613.
42. Alexiou, C.; Arnold, W.; Klein, R. J.; Parak, F. G.; Hulin, P.; Bergemann, C.; Erhardt, W.; Wagenpfeil, S.; Lubbe, A. S. Locoregional Cancer Treatment with Magnetic Drug Targeting. *Cancer Res.* **2000**, *60*, 6641–6648.
43. Namiki, Y.; Namiki, T.; Yoshida, H.; Ishii, Y.; Tsubota, A.; Koido, S.; Nariai, K.; Mitsunaga, M.; Yanagisawa, S.; Kashiwagi, H.; et al. A Novel Magnetic Crystal-Lipid Nanostructure for Magnetically Guided *in Vivo* Gene Delivery. *Nat. Nanotechnol.* **2009**, *4*, 598–606.
44. Yezhelyev, M. V.; Qi, L.; O'Regan, R. M.; Nie, S.; Gao, X. Proton-Sponge Coated Quantum Dots for Sirna Delivery and Intracellular Imaging. *J. Am. Chem. Soc.* **2008**, *130*, 9006–9012.
45. Ding, H.-m.; Ma, Y.-q. Role of Physicochemical Properties of Coating Ligands in Receptor-Mediated Endocytosis of Nanoparticles. *Biomaterials* **2012**, *33*, 5798–5802.
46. Torchilin, V. P.; Trubetskoy, V. S. Which Polymers Can Make Nanoparticulate Drug Carriers Long-Circulating? *Adv. Drug Delivery Rev.* **1995**, *16*, 141–155.
47. Tromsdorf, U. I.; Bigall, N. C.; Kaul, M. G.; Bruns, O. T.; Nikolic, M. S.; Mollwitz, B.; Sperling, R. A.; Reimer, R.; Hohenberg, H.; Parak, W. J.; et al. Size and Surface Effects on the Mri Relaxivity of Manganese Ferrite Nanoparticle Contrast Agents. *Nano Lett.* **2007**, *7*, 2422–2427.
48. Silverstein, S. C.; Steinman, R. M.; Cohn, Z. A. Endocytosis. *Annu. Rev. Biochem.* **1977**, *46*, 669–722.
49. Goldstein, J. L.; Anderson, R. G. W.; Brown, M. S. Coated Pits, Coated Vesicles, and Receptor-Mediated Endocytosis. *Nature* **1979**, *279*, 679–685.
50. Blanchard, E.; Belouzard, S.; Goueslain, L.; Wakita, T.; Dubuisson, J.; Wychowski, C.; Rouille, Y. Hepatitis C Virus Entry Depends on Clathrin-Mediated Endocytosis. *J. Virol.* **2006**, *80*, 6964–6972.
51. Dimitrov, D. S. Virus Entry: Molecular Mechanisms and Biomedical Applications. *Nat. Rev. Microbiol.* **2004**, *2*, 109–122.
52. Gruenberg, J.; van der Goot, F. G. Mechanisms of Pathogen Entry through the Endosomal Compartments. *Nat. Rev. Mol. Cell Biol.* **2006**, *7*, 495–504.
53. Lerner, D. M.; Deutsch, J. M.; Oster, G. F. How Does a Virus Bud. *Biophys. J.* **1993**, *65*, 73–79.
54. Garoff, H.; Hewson, R.; Opstelten, D. J. E. Virus Maturation by Budding. *Microbiol. Mol. Biol. Rev.* **1998**, *62*, 1171–1190.
55. Nel, A. E.; Maedler, L.; Velegol, D.; Xia, T.; Hoek, E. M. V.; Somasundaran, P.; Klaessig, F.; Castranova, V.; Thompson, M. Understanding Biophysicochemical Interactions at the Nano-Bio Interface. *Nat. Mater.* **2009**, *8*, 543–557.
56. Decuzzi, P.; Ferrari, M. The Role of Specific and Non-Specific Interactions in Receptor-Mediated Endocytosis of Nanoparticles. *Biomaterials* **2007**, *28*, 2915–2922.
57. Gao, H.; Shi, W.; Freund, L. B. Mechanics of Receptor-Mediated Endocytosis. *Proc. Natl. Acad. Sci. U. S. A.* **2005**, *102*, 9469–9474.
58. Bao, G.; Bao, X. R. Shedding Light on the Dynamics of Endocytosis and Viral Budding. *Proc. Natl. Acad. Sci. U. S. A.* **2005**, *102*, 9997–9998.
59. Zhang, S. L.; Zhu, T.; Belytschko, T. Atomistic and Multiscale Analyses of Brittle Fracture in Crystal Lattices. *Phys. Rev. B: Condens. Matter Mater. Phys.* **2007**, *76*, 094114.
60. Terdalkar, S. S.; Yuan, H. Y.; Huang, S.; T, Z.; Rencis, J. J.; Zhang, S. L. Nanoscale Fracture in Graphene. *Chem. Phys. Lett.* **2010**, *494*, 218–222.
61. Freund, L. B.; Lin, Y. The Role of Binder Mobility in Spontaneous Adhesive Contact and Implications for Cell Adhesion. *J. Mech. Phys. Solids* **2004**, *52*, 2455–2472.
62. Shenoy, V. B.; Freund, L. B. Growth and Shape Stabillity of a Biological Membrane Adhesion Complex in the Diffusion-Mediated Regime. *Proc. Natl. Acad. Sci. U. S. A.* **2005**, *102*, 3213–3218.
63. Tzlil, S.; Deserno, M.; Gelbert, W. M.; Ben-Shaul, A. A Statistical-Thermodynamic Model of Viral Budding. *Biophys. J.* **2004**, *86*, 2037–2048.
64. Zhang, S. L.; Li, J.; Lykotrafitis, G.; Bao, G.; Suresh, S. Size-Dependent Endocytosis of Nanoparticles. *Adv. Mater.* **2009**, *21*, 419–424.
65. Yuan, H. Y.; Li, J.; Bao, G.; Zhang, S. Variable Adhesion Strength Regulates Cellular Uptake. *Phys. Rev. Lett.* **2010**, *105*, 138101.

66. Yuan, H. Y.; Zhang, S. L. Effects of Particle Size and Ligand Density on the Kinetics of Receptor-Mediated Endocytosis of Nanoparticles. *Appl. Phys. Lett.* **2010**, *96*, 033704.
67. Kosmalska, A. J.; Casares, L.; Elosegui-Artola, A.; Thottacherry, J. J.; Moreno-Vicente, R.; Gonzalez-Tarrago, V.; del Pozo, M. A.; Mayor, S.; Arroyo, M.; Navajas, D.; et al. Physical Principles of Membrane Remodelling During Cell Mechanoadaptation. *Nat. Commun.* **2015**, *6*, 7292.
68. Deserno, M.; Bickel, T. Wrapping of a Spherical Colloid by a Fluid Membrane. *Europhys. Lett.* **2003**, *62*, 767–773.
69. Deserno, M. Elastic Deformation of a Fluid Membrane Upon Colloid Binding. *Phys. Rev. E* **2004**, *69*, 031903.
70. Reynwar, B. J.; Illya, G.; Harmandaris, V. A.; Muller, M. M.; Kremer, K.; Deserno, M. Aggregation and Vesiculation of Membrane Proteins by Curvature-Mediated Interactions. *Nature* **2007**, *447*, 461–464.
71. Chithrani, B. D.; Ghazani, A. A.; Chan, W. C. W. Determining the Size and Shape Dependence of Gold Nanoparticle Uptake into Mammalian Cells. *Nano Lett.* **2006**, *6*, 662–668.
72. Dietrich, C.; Angelova, M.; Pouligny, B. Adhesion of Latex Spheres to Giant Phospholipid Vesicles: Statics and Dynamics. *J. Phys. II* **1997**, *7*, 1651–1682.
73. Aoyama, Y.; Kanamori, T.; Nakai, T.; Sasaki, T.; Horiuchi, S.; Sando, S.; Niidome, T. Artificial Viruses and Their Application to Gene Delivery. Size-Controlled Gene Coating with Glycocluster Nanoparticles. *J. Am. Chem. Soc.* **2003**, *125*, 3455–3457.
74. Osaki, F.; Kanamori, T.; Sando, S.; Sera, T.; Aoyama, Y. A Quantum Dot Conjugated Sugar Ball and Its Cellular Uptake on the Size Effects of Endocytosis in the Subviral Region. *J. Am. Chem. Soc.* **2004**, *126*, 6520–6521.
75. Chithrani, B. D.; Chan, W. C. W. Elucidating the Mechanism of Cellular Uptake and Removal of Protein-Coated Gold Nanoparticles of Different Sizes and Shapes. *Nano Lett.* **2007**, *7*, 1542–1550.
76. Xing, X. L.; He, X. X.; Peng, J. F.; Wang, K. M.; Tan, W. H. Uptake of Silica-Coated Nanoparticles by Hela Cells. *J. Nanosci. Nanotechnol.* **2005**, *5*, 1688–1693.
77. Lamblet, M.; Delord, B.; Johannes, L.; van Effenterre, D.; Bassereau, P. Key Role of Receptor Density in Colloid/Cell Specific Interaction: A Quantitative Biomimetic Study on Giant Vesicles. *Eur. Phys. J. E: Soft Matter Biol. Phys.* **2008**, *26*, 205–216.
78. van Effenterre, D.; Roux, D. Adhesion of Colloids on a Cell Surface in Competition for Mobile Receptors. *Europhys. Lett.* **2003**, *64*, 543–549.
79. Yuan, H. Y.; Huang, C. J.; Zhang, S. L. Virus-Inspired Design Principles of Nanoparticle-Based Bioagents. *PLoS One* **2010**, *5*, e13495.
80. Garoff, H.; Simons, K. Location of Spike Glycoproteins in Semliki Forest Virus Membrane. *Proc. Natl. Acad. Sci. U. S. A.* **1974**, *71*, 3988–3992.
81. Strauss, J. H.; Strauss, E. G. The Alphaviruses: Gene-Expression, Replication, and Evolution. *Microbiol. Rev.* **1994**, *58*, 491–562.
82. Sun, S. X.; Wirtz, D. Mechanics of Enveloped Virus Entry into Host Cells. *Biophys. J.* **2006**, *90*, L10–L12.
83. Huang, C. J.; Zhang, Y.; Yuan, H. Y.; Gao, H. J.; Zhang, S. L. Role of Nanoparticle Geometry in Endocytosis: Laying Down to Stand Up. *Nano Lett.* **2013**, *13*, 4546–4550.
84. Shi, X. H.; von dem Bussche, A.; Hurt, R. H.; Kane, A. B.; Gao, H. J. Cell Entry of One-Dimensional Nanomaterials Occurs by Tip Recognition and Rotation. *Nat. Nanotechnol.* **2011**, *6*, 714–719.
85. Li, Y. F.; Yuan, H. Y.; von dem Bussche, A.; Creighton, M.; Hurt, R. H.; Kane, A. B.; Gao, H. J. Graphene Microsheets Enter Cells through Spontaneous Membrane Penetration at Edge Asperities and Corner Sites. *Proc. Natl. Acad. Sci. U. S. A.* **2013**, *110*, 12295–12300.
86. Yi, X.; Gao, H. J. Phase Diagrams and Morphological Evolution in Wrapping of Rod-Shaped Elastic Nanoparticles by Cell Membrane: A Two-Dimensional Study. *Phys. Rev. E* **2014**, *89*, 062712.
87. Yi, X.; Gao, H. J. Cell Interaction with Graphene Microsheets: Near-Orthogonal Cutting Versus Parallel Attachment. *Nanoscale* **2015**, *7*, 5457–5467.
88. Yi, X.; Shi, X. H.; Gao, H. J. A Universal Law for Cell Uptake of One-Dimensional Nanomaterials. *Nano Lett.* **2014**, *14*, 1049–1055.
89. Atilgan, E.; Sun, S. X. Shape Transitions in Lipid Membranes and Protein Mediated Vesicle Fusion and Fission. *J. Chem. Phys.* **2007**, *126*, 095102.
90. Noguchi, H.; Gompper, G. Shape Transitions of Fluid Vesicles and Red Blood Cells in Capillary Flows. *Proc. Natl. Acad. Sci. U. S. A.* **2005**, *102*, 14159–14164.
91. Helfrich, W. Elastic Properties of Lipid Bilayers - Theory and Possible Experiments. *Z. Naturforsch., C: J. Biosci.* **1973**, *28*, 693–703.
92. Lyubartsev, A. P. Multiscale Modeling of Lipids and Lipid Bilayers. *Eur. Biophys. J.* **2005**, *35*, 53–61.
93. Cooke, I. R.; Deserno, M. Solvent-Free Model for Self-Assembling Fluid Bilayer Membranes: Stabilization of the Fluid Phase Based on Broad Attractive Tail Potentials. *J. Chem. Phys.* **2005**, *123*, 224710.
94. Cooke, I. R.; Kremer, K.; Deserno, M. Tunable Generic Model for Fluid Bilayer Membranes. *Phys. Rev. E* **2005**, *72*, 011506.
95. Yuan, H. Y.; Huang, C. J.; Li, J.; Lykotrafitis, G.; Zhang, S. L. One-Particle-Thick, Solvent-Free, Coarse-Grained Model for Biological and Biomimetic Fluid Membranes. *Phys. Rev. E* **2010**, *82*, 011905.
96. Drouffe, J. M.; Maggs, A. C.; Leibler, S. Computer-Simulations of Self-Assembled Membranes. *Science* **1991**, *254*, 1353–1356.
97. Yamamoto, S.; Maruyama, Y.; Hyodo, S. Dissipative Particle Dynamics Study of Spontaneous Vesicle Formation of Amphiphilic Molecules. *J. Chem. Phys.* **2002**, *116*, 5842–5849.
98. Brannigan, G.; Philips, P. F.; Brown, F. L. H. Flexible Lipid Bilayers in Implicit Solvent. *Phys. Rev. E* **2005**, *72*, 011915.
99. Noguchi, H.; Gompper, G. Meshless Membrane Model Based on the Moving Least-Squares Method. *Phys. Rev. E* **2006**, *73*, 021903.
100. Marrink, S. J.; Risselada, H. J.; Yefimov, S.; Tieleman, D. P.; de Vries, A. H. The Martini Force Field: Coarse Grained Model for Biomolecular Simulations. *J. Phys. Chem. B* **2007**, *111*, 7812–7824.
101. Yuan, H.; Huang, C.; Zhang, S. Dynamic Shape Transformations of Fluid Vesicles. *Soft Matter* **2010**, *6*, 4571–4579.
102. Huang, C. J.; Yuan, H. Y.; Zhang, S. L. Coupled Vesicle Morphogenesis and Domain Organization. *Appl. Phys. Lett.* **2011**, *98*, 043702.
103. Li, H.; Lykotrafitis, G. A Coarse-Grain Molecular Dynamics Model for Sickle Hemoglobin Fibers. *J. Mech. Behav. Biomed. Mater.* **2011**, *4*, 162–173.
104. Zhang, Y.; Huang, C. J.; Kim, S.; Golkaram, M.; Dixon, M. W.; Tilley, L.; Li, J.; Zhang, S. L.; Suresh, S. Multiple Stiffening Effects of Nano-Scale Knobs on Human Red Blood Cells Infected with Plasmodium Falciparum Malaria Parasite. *Proc. Natl. Acad. Sci. U. S. A.* **2015**, *112*, 6068–6073.
105. Vacha, R.; Martinez-Veracoechea, F. J.; Frenkel, D. Receptor-Mediated Endocytosis of Nanoparticles of Various Shapes. *Nano Lett.* **2011**, *11*, 5391–5395.
106. Yi, X.; Shi, X. H.; Gao, H. J. Cellular Uptake of Elastic Nanoparticles. *Phys. Rev. Lett.* **2011**, *107*, 098101.
107. Sun, J. S.; Zhang, L.; Wang, J. L.; Feng, Q.; Liu, D. B.; Yin, Q. F.; Xu, D. Y.; Wei, Y. J.; Ding, B. Q.; Shi, X. H.; et al. Tunable Rigidity of (Polymeric Core)-(Lipid Shell) Nanoparticles for Regulated Cellular Uptake. *Adv. Mater.* **2015**, *27*, 1402–1407.
108. Yi, X.; Gao, H. J. Cell Membrane Wrapping of a Spherical Thin Elastic Shell. *Soft Matter* **2015**, *11*, 1107–1115.
109. Jiang, W.; KimBetty, Y. S.; Rutka, J. T.; ChanWarren, C. W. Nanoparticle-Mediated Cellular Response Is Size-Dependent. *Nat. Nanotechnol.* **2008**, *3*, 145–150.

110. Jun, Y.-w.; Huh, Y.-M.; Choi, J.-s.; Lee, J.-H.; Song, H.-T.; Kim, K.; Yoon, S.; Kim, K.-S.; Shin, J.-S.; Suh, J.-S.; et al. Nanoscale Size Effect of Magnetic Nanocrystals and Their Utilization for Cancer Diagnosis *via* Magnetic Resonance Imaging. *J. Am. Chem. Soc.* **2005**, *127*, 5732–5733.
111. Bershadsky, A. D.; Balaban, N. Q.; Geiger, B. Adhesion-Dependent Cell Mechanosensitivity. *Annu. Rev. Cell Dev. Biol.* **2003**, *19*, 677–695.
112. Pelham, R. J.; Wang, Y. L. Cell Locomotion and Focal Adhesions Are Regulated by Substrate Flexibility. *Proc. Natl. Acad. Sci. U. S. A.* **1997**, *94*, 13661–13665.
113. Vogel, V.; Sheetz, M. Local Force and Geometry Sensing Regulate Cell Functions. *Nat. Rev. Mol. Cell Biol.* **2006**, *7*, 265–275.
114. Wang, N.; Butler, J. P.; Ingber, D. E. Mechanotransduction across the Cell Surface and through the Cytoskeleton. *Science* **1993**, *260*, 1124–1127.
115. Wozniak, M. A.; Chen, C. S. Mechanotransduction in Development: A Growing Role for Contractility. *Nat. Rev. Mol. Cell Biol.* **2009**, *10*, 34–43.
116. Hamill, O. P.; Martinac, B. Molecular Basis of Mechanotransduction in Living Cells. *Physiol. Rev.* **2001**, *81*, 685–740.
117. Huang, C. J.; Butler, P. J.; Tong, S.; Muddana, H. S.; Bao, G.; Zhang, S. L. Substrate Stiffness Regulates Cellular Uptake of Nanoparticles. *Nano Lett.* **2013**, *13*, 1611–1615.
118. Huang, C. J.; Ozdemir, T.; Xu, C.; Butler, P. J.; Siedlecki, C.; Brown, J. L.; Zhang, S. L. The Role of Substrate Topography on the Cellular Uptake of Nanoparticles. *J. Biomed. Mater. Res., Part B* **2015**, 10.1002/jbm.b.33397.
119. Muddana, H. S.; Gullapalli, R. R.; Manias, E.; Butler, P. J. Atomistic Simulation of Lipid and Dii Dynamics in Membrane Bilayers under Tension. *Phys. Chem. Chem. Phys.* **2011**, *13*, 1368–1378.
120. Tabouillot, T.; Muddana, H. S.; Butler, P. J. Endothelial Cell Membrane Sensitivity to Shear Stress Is Lipid Domain Dependent. *Cell. Mol. Bioeng.* **2011**, *4*, 169–181.